MethodsX 13 (2024) 103062

Contents lists available at ScienceDirect

MethodsX

journal homepage: www.elsevier.com/locate/methodsx

Design and evaluation of an open-source block face imaging system for 2D histology to magnetic resonance image registration ☆

Mingzhen Shao [a,*], Amanpreet Singh [a], Sara Johnson [b], Alissa Pessin [b], Robb Merrill [b], Ariana Page [b], Henrik Odéen [b], Sarang Joshi [c], Allison Payne [b]

[a] *Kahlert School of Computing, Scientific Computing and Imaging Institute, University of Utah, 72 S Central Campus Drive, Salt Lake City, UT, 84112, USA*

[b] *Department of Radiology and Imaging Sciences, University of Utah, 729 Arapeen Drive, Salt Lake City, UT, 84109, USA*

[c] *Biomedical Engineering Department, Scientific Computing and Imaging Institute, University of Utah, 72 S Central Campus Drive, Salt Lake City, UT, 84112, USA*

ARTICLE INFO

Method name:
Registration of 2D histology images to magnetic resonance images

Keywords:
Histology registration
Focused ultrasound
Block face imaging

ABSTRACT

This study introduces a comprehensive hardware-software framework designed to enhance the quality of block face image capture—an essential intermediary step for registering 2D histology images to ex vivo magnetic resonance (MR) images. A customized camera mounting and lighting system is employed to maintain consistent relative positioning and lighting conditions. Departing from traditional transparent paraffin, dyed paraffin is utilized to enhance contrast for subsequent automatic segmentation. Our software facilitates fully automated data collection and organization, complemented by a real-time Quality Assurance (QA) section to assess the captured image's quality during the sectioning process. The setup is evaluated and validated using rabbit muscle and rat brain which underwent MR-guided focused ultrasound ablations. The customized hardware system establishes a robust image capturing environment. The software with a real-time QA section, enables operators to promptly rectify low-quality captures, thereby preventing data loss. The execution of our proposed framework produces robust registration results for H&E images to ex vivo MR images.

- The presented hardware-software framework ensures the uniformity and resilience of the block face image capture process, contributing to a more reliable and efficient registration of 2D histology images to ex vivo MR images.

☆ ***For a published article:*** B. E. Zimmerman, S. L. Johnson, H. A. Odéen, J. E. Shea, R. E. Factor, S. C. Joshi, and A. H. Payne, "Histology to 3D in vivo MR registration for volumetric evaluation of MRgFUS treatment assessment biomarkers," Scientific Reports, vol. 11, no.1, p.18923, 2021.

* Corresponding author.
E-mail address: shao@cs.utah.edu (M. Shao).

https://doi.org/10.1016/j.mex.2024.103062
Received 18 September 2024; Accepted 16 November 2024
Available online 20 November 2024

Specifications table

Subject area:	Medicine and Dentistry
More specific subject area:	Medical Image Registration
Name of your method:	Registration of 2D histology images to magnetic resonance images
Name and reference of original method:	B. E. Zimmerman, S. L. Johnson, H. A. Odéen, J. E. Shea, R. E. Factor, S. C. Joshi, and A. H. Payne, "Histology to 3D in vivo MR registration for volumetric evaluation of MRgFUS treatment assessment biomarkers," Scientific Reports, vol. 11, no.1, p.18923, 2021
Resource availability:	https://github.com/fuslab-uofu/RecordingGUI

Background

Advances in imaging and early cancer detection have increased interest in minimally and non-invasive cancer treatment options, including non-invasive magnetic resonance guided focused ultrasound (MRgFUS) technologies. MRgFUS provides several potential advantages over traditional surgical approaches including real time image guidance, the ability to treat patients who are not good surgical candidates [1], reduction of operation pain and shortened recovery time.

Because MRgFUS is applied non-invasively and the treated tumor is ideally not resected, imaging biomarkers must determine treatment efficacy [2]. While MR image guidance can provide patient-specific treatment planning, real-time monitoring and assessment, MRI currently does not provide enough information about the cancer state to ensure treatment efficacy [2–5]. Therefore, the ability to precisely compare between in vivo MRI derived biomarkers and 2D histology images is a key need for MRgFUS and other non-invasive technologies.

Several methods in the literature have attempted to restore the spatial relationship between in vivo diagnostic or treatment-evaluation MR images and 2D histology imaging [6–16]. However, all these registration methods rely on features that correlate directly between in vivo MR images and histology that are independent of the diagnostic or treatment features being evaluated [9]. In numerous MRgFUS ablation applications, such as those involving the liver, breast, or kidney, ancillary features like bone and blood vessels, which are independent of the ablation treatment itself, are often unavailable for incorporation into the registration process. The potential lack of sufficient correlating features between in vivo MR and histology independent of the treatment features prohibits using these registration methods.

To solve this problem, Zimmerman et al. [17] proposed a new tissue based registration method that uses the ex vivo tissue as an intermediate stage to register the MR images to the histology images. Instead of directly registering the histology images to the in vivo MR images, this method collects both ex vivo MR images and block face images before tissue sectioning to capture the deformations of both the tissue excision and microtome processes. As described in their work, the intermediate ex vivo tissue imaging steps are a very important component of the registration technique when dealing with tissues that do not have sufficient correlating features between in vivo MRI and histology.

While the feasibility of this new technique was demonstrated, the ex vivo imaging techniques, particularly the block face image acquisition, was not robustly designed to enable high data throughput and minimize user errors. These are vital steps of the overall process as multiple histology blocks are often processed for a single subject, and due to the destructive nature of tissue sectioning, undetected user errors can result in substantial loss of irreplaceable data.

This methods paper describes an advanced block face imaging system that addresses these limitations. The system comprises a customized hardware and software design, ensuring consistency while simplifying the block face tissue segmentation process. The integration of these hardware and software components facilitates accurate, high throughput in vivo MRI to histology registration, providing a robust and efficient solution to MRI to 2D histology registration.

Method details

The block face imaging system incorporates numerous features that ensures consistency in environmental variables, enhances focusing precision, and simplifying the block face tissue segmentation process. Importantly, the customized software includes a built-in quality assessment feature, assuring the accuracy and consistency of the acquired data. The acquisition software, room layout, equipment and parts list are detailed below.

Overview of required hardware and siting

The design of hardware and siting of the different equipment needs took into account several key features, including consistent control of lighting and robust equipment positioning. To avoid environmental lighting inconsistencies, the sectioning room is sealed off from external light sources through completely covering windows and door openings with black-out curtains. Both the camera and lighting systems are securely mounted on the wall and positioned to directly face the microtome for optimal image capture. The computer that controls image acquisition and data processing is located immediately adjacent to other equipment, enabling operators to receive real-time quality assurance during the collection process. Fig. 1 shows both a schematic and photographic overview of the image collection room.

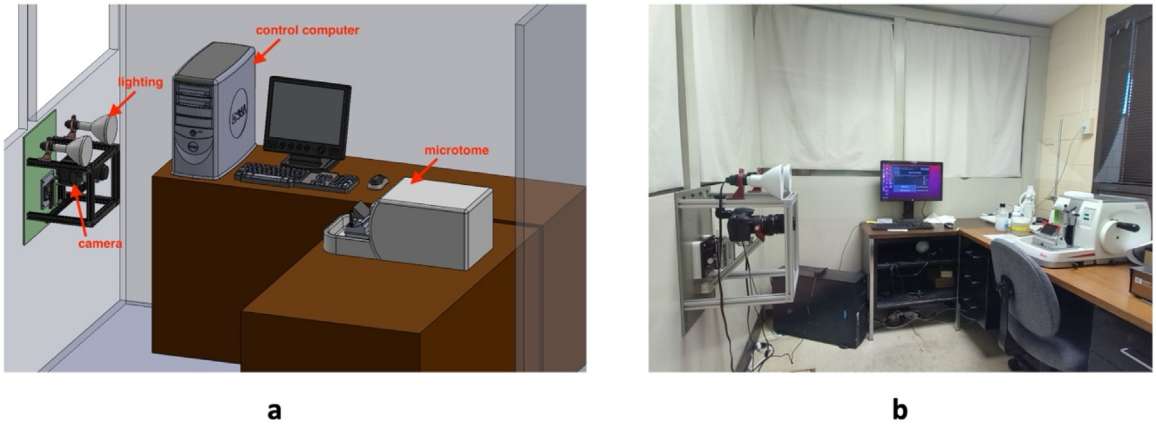

Fig. 1. Overview of the histology section room. (a) Sectioning room layout schematic. The camera, lighting, control computer and microtome are labeled. (b) Photograph of the section room showing the window coverings and functional layout.

Camera mounting

Fig. 2 shows the custom camera mount designed to keep the relative camera position fixed and to protect the camera system. The camera is securely mounted on an XY stage (TECHSPEC, NJ, USA) which is attached to the wall surface and precisely aligned to capture images of the block face, allowing for accurate and stable adjustments in two dimensions along the wall surface, with an approximate adjustment range of ±30mm in each direction. The XY stage is employed for precise adjustments, ensuring that the lens axis remains constantly aligned with the block face, allowing for optimal imaging and analysis. The frame of the camera holder is designed to protect the camera and provide mounting points for the LED lights, described below.

Lighting

Consistent lighting is a crucial requirement for the acquisition process. To prevent environmental lighting disturbances and to maintain consistency throughout the acquisition process, we placed the collection system in a darkroom, relying solely on artificial lights. These lights include the overhead room light and an LED lighting system integrated with our capture system.

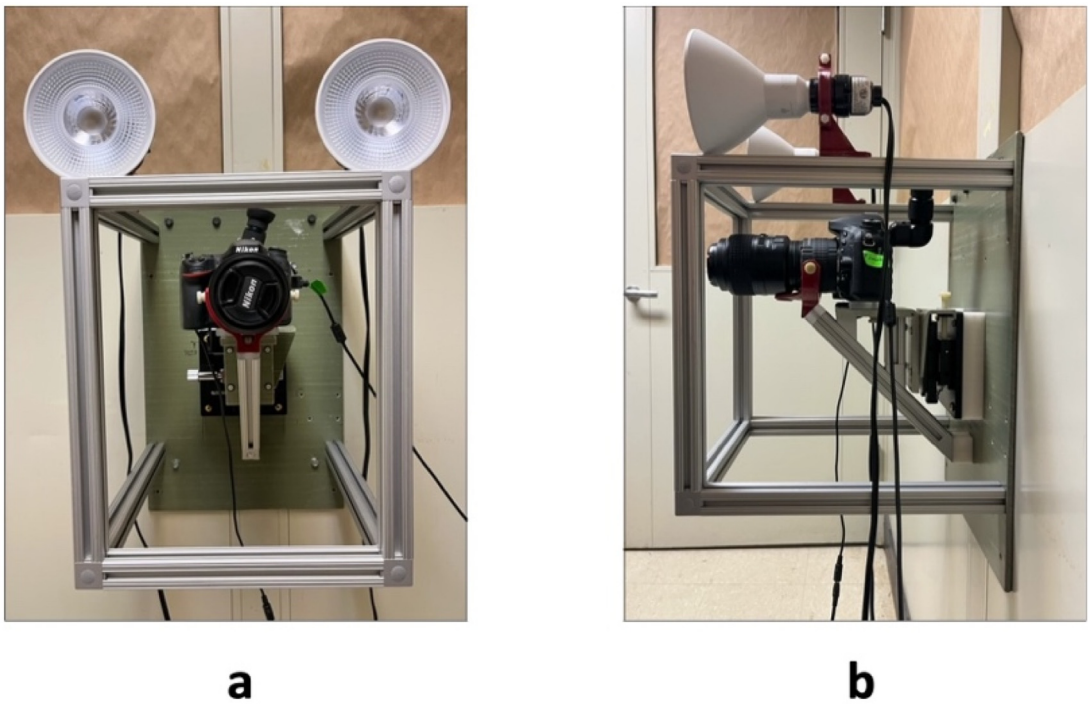

Fig. 2. Picture of camera assembly mounted to the wall of the sectioning room. Camera is surrounded by a protective frame to prevent accidental bumps. Lighting is mounted to the protective frame. Both (a) front and (b) side views are shown.

The overhead light provides necessary illumination during sectioning and capturing surface images. The LED lighting system is responsible for scatter illumination during the capture of scatter images. This system consists of an Arduino (Uno R3) and two 1200-lumen LED lights (PAR38 17 W, Bluex Bulbs). The capture program instructs the Arduino to control different lights based on the specific images being captured.

Tissue preparation

Tissue inking to maintain orientation

After excision, removed tissue undergoes a meticulous marking process using pathology inks. This ensures the preservation of MR orientation throughout various stages of gross tissue harvest and processing. While this work has evaluated animal tissues harvested from euthanized subjects, these techniques could be adapted to different pathology gross room practices. Each face of the excised tissue is distinctly marked with a specific color to signify its orientation: red for patient's right side, black for patient's left side, yellow for the foot (inferior), green for the head (superior), and blue for the top surface (as seen in Fig. 3a). Following inking, the tissue is fixed for 7 days in formalin.

Agar embedding of tissue

The formalin-fixed tissues requires agar embedding for ex vivo imaging and gross tissue slicing. The agar, serving as a critical boundary and signal source, ensures adequate conditions for high-resolution ex vivo MR imaging, such as reducing motion of surrounding medium and the tissue itself, and maintains the stability and orientation of the tissue during gross slicing.

The agar embedding is performed in three key steps. First, the tissue sample is carefully positioned, maintaining orientation, in a custom tissue embedding box, and six-eight stabilizing prongs are placed around the container to provide support for the sample (Fig. 3a). Second, the embedding box is filled with an 2.5 % agar (Sigma Aldrich, Burlington, MA) gel solution in deionized water. The solution is poured just below the height of the stabilizing prongs, avoiding the collection of air bubbles beneath the tissue (Fig. 3b). Once the agar solution partially sets (approximately 15 min in a 4 ˚C fridge), the prongs are gently retracted, leaving the tissue

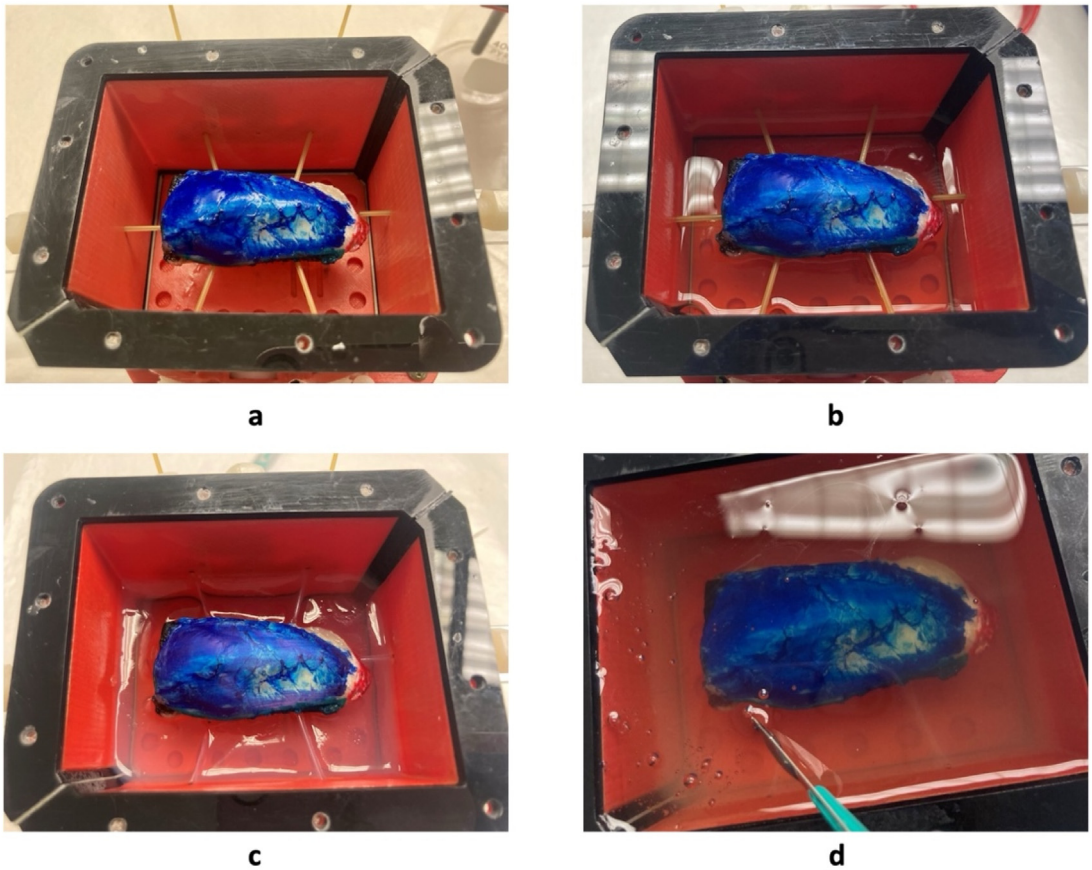

Fig. 3. Agar embedding steps for the excised tissue. (a) Inked, excised tissue placed in embedding box with stabilizing prongs. (b) Partial agar solution fill to base of stabilizing prongs. (c) Agar solution fill after stabilizing prongs are removed. (d) Manual removal of bubbles that form during the agar pour.

securely embedded in the partially set agar (Fig. 3c). Finally, a second layer of agar is poured over the remaining tissue, with careful removal of bubbles (Fig. 3d). This comprehensive process ensures the integrity of the tissue structure and its readiness for subsequent imaging and slicing procedures.

Tissue grossing

The grossing process facilitates the slicing of tissue into thin layers, making it easily processable and ready for sectioning. We use a deli slicer (Backyard Pro SL112E) to achieve precise 3 mm thickness of the slices and to reduce the necessary force required to slice the tissue [18]. Slice thickness is confirmed via caliper measurement. Following the slicing, the tissue is carefully removed from the agar and placed in a tissue cassette.

Paraffin embedding for sectioning

The registration pipeline necessitates the segmentation of tissue edges from the surrounding paraffin. However, clear paraffin presents a significant challenge due to its low contrast around the tissue, making it difficult to differentiate between the tissue and the paraffin background.

The tissue is generally a warm neutral color. Therefore, to enhance contrast at the tissue boundary, a color complementary to the tissue's warm neutral tone should be used. Theoretically, the best choice would be the blue color on the opposite side of the color wheel should be used. After considering the accessibility of various dye options, we've opted for a dark blue background. This choice aims to increase contrast between the tissue edge and paraffin, ensuring the tissue stands out distinctly, while also addressing the transparency issue associated with clear paraffin. Paraffin coloring was achieved by adding 14 drops of blue dye and 2 drops of black dye (Lone Star Blue/Sky Blue and Black/Gray Liquid Dye, Lone Star Candle Supply, Inc., Keller TX, USA) to 2 pounds of paraffin (EprediaTM Paraffin Type 9).

Fig. 4 compares the captured paraffin block face images with undyed and dark blue colored paraffin. Qualitatively, there is a substantially enhanced contrast between the non-dyed and dark blue paraffin surrounds.

Tissue sectioning protocol

Sectioning protocol

Tissue blocks were sectioned with a microtome (RM2255, Leica Microsystems, Wetzlar, Germany) at 10 um increments. Digital images of the block face were acquired every 50 um starting from the very beginning of the block using a digital single-lens reflex (DSLR) camera (Nikon D7100; Macro 1:1 105 mm Lens; 2.0x teleconverter). The image size and approximate resolution for a block face image were 6000 × 4000 with ~0.023 mm isotropic spacing. The camera shutter was controlled by the program gphoto2. Captured images were transferred in real time to the sectioning computer using a USB cable.

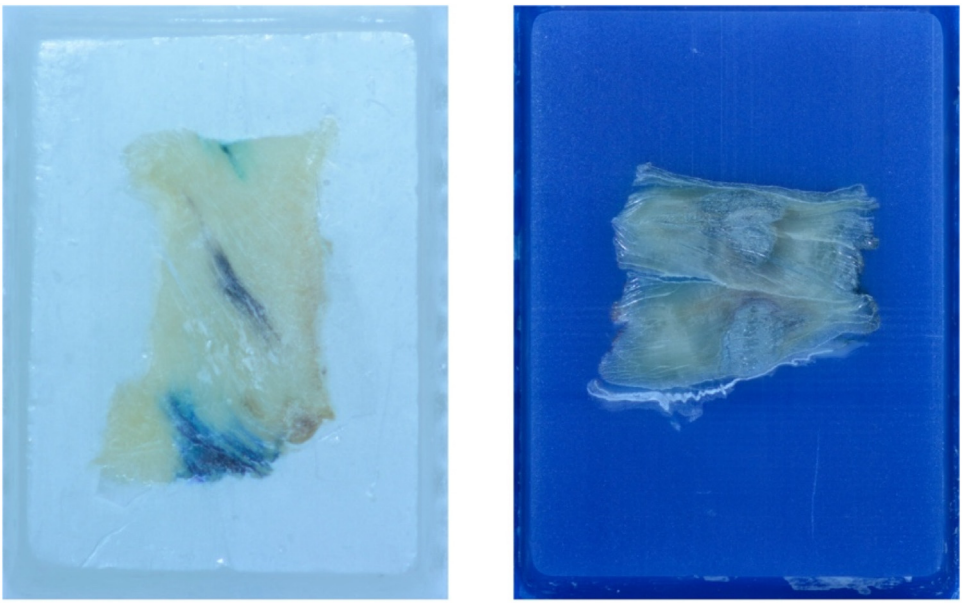

Fig. 4. Comparison between non-dyed and colored paraffin with embedded tissues (left: non-dyed paraffin, right: colored paraffin with dark blue dye). It was determined the dark blue dye (right) provided sufficient contrast for segmentation.

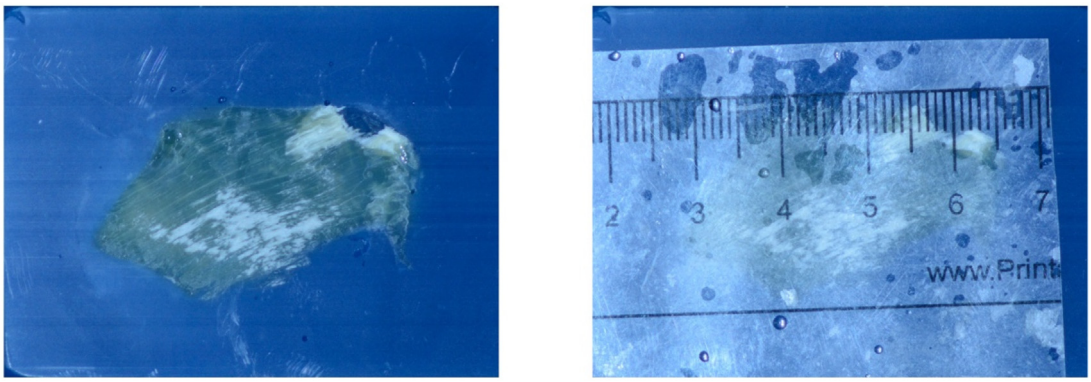

Fig. 5. Comparison of contrast between a standard block and a block with a ruler (left: standard block, right: block with a ruler). It was determined that the ruler provided sufficient contrast for checking focus status.

Camera focusing protocol

Achieving accurate camera focus is crucial, directly influencing the quality of the acquired block face image. The smooth surface of the blocks lack texture, posing a challenge for assessing focus. To address this, a ruler with millimeter markings is affixed to the block's face at the beginning of the sectioning procedure, providing the necessary contrast for the focus procedure.

For manual focusing, an angle viewer is employed, allowing users to adjust focus manually, by eye. In Fig. 5, two captures are presented—one with a ruler sticker and one without. The presence of the ruler sticker makes it easier to discern the focus status.

Image acquisition software

Tissue sectioning is a destructive process. Therefore, it is critical that the image acquisition software is designed to provide the user the ability to perform sufficient quality control checks to ensure the data is of the standard required to perform registration between the sectioned tissue and the acquired block face image.

The proposed software can be divided into three key components:

- Main window
- Image window
- Center point window

The work flow overview of the image acquisition software is illustrated in Fig. 6.

Upon launching the application, a port connection check is performed to ensure proper functionality and connectivity of the LED lighting system and camera. After completing the connection check, the program launches the main window, providing access to the acquisition settings. Operators can use the main window to configure the primary and backup storage locations, adjust camera capture settings, and specify the distance information for the block face images.

Once an image is captured, the program automatically launches the image window that displays the captured image, along with any segmentation results (see below). Operators can then refine the segmentation results and evaluate the quality of the capture. This window also enables operators to provide section information and add notes for future reference. Based on their assessment, the operators can either accept or retake the capture.

Upon capturing the initial image for a particular block, an automated launch of the center point window takes place. Within this window, operators are prompted to pinpoint the center of the block face image. This identification plays a crucial role in isolating the block face from the background. The subsequent reduction of unnecessary data enhances segmentation speed and accuracy. Detailed instructions for each part are provided in the following sections.

Main window

The "Main Window" can be divided into six functional parts (numbered in Fig. 7).

1. **Folder setting:** Operators provide the block's name and use the "generate path" button to generate the primary and backup storage locations for data.
2. **Capture button:** This button triggers the capture image process.
3. **State information:** The program's current state will be shown here. It is used to interact with the operators. Detailed information will be shown here if any errors occur, or external operations are needed. Otherwise, it will show "Everything Normal".
4. **List of captured images:** All captured images in the saving folder will be listed with the associated information.
5. **Exposure setting:** Operators can adjust the exposure setting for different captures (surface and scatter). By providing different ISO, f/stop, and shutter speed settings, the operators can get images with different brightness and depth of field.
6. **Distance setting:** There are two thickness options for each section: 50 um or 5 um. Operators must select the correct distance based on their section before a capture process, and the distance will be associated with the captured images.

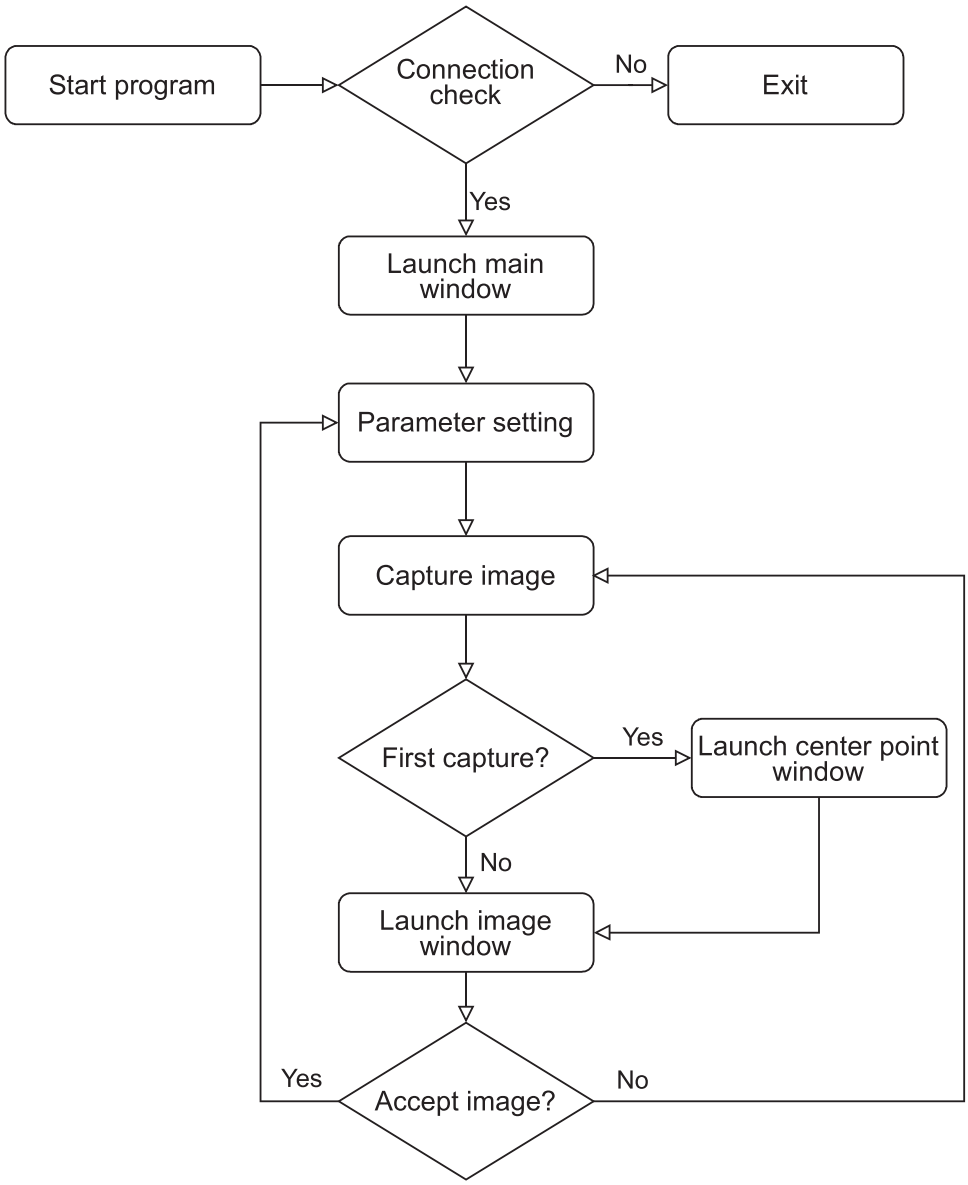

Fig. 6. Work flow overview of the block face imaging capture software.

Image window

The "Image Window" is launched after each capture and can be divided into four distinct parts, as illustrated in Fig. 8.

1. **Capture confirmation:** After assessing the segmentation results, the operator decides to accept this capture and proceed, or they can redo the capture to correct any mistakes. The operator can also add notes for future reference.
2. **Segmentation operation:** The operator can use these buttons to manually select patches to provide the necessary information for the Linear Discriminant Analysis (LDA) segmentation. If not manually selected, default patches are implemented. The outputs of the segmentation process can vary depending on the selection of different patches.
3. **Capture results:** The captured surface and scatter images are shown here.
4. **Segmentation results:** The cropped scatter image and segmentation result are shown here. The operator needs to assess if the segmentation result adequately represents the tissue state.

Center point window

During the initial capture for each block, the center point window will be automatically launched. In this window, the operator is required to manually provide the center point of the block. This information will be used in the subsequent crop and segmentation

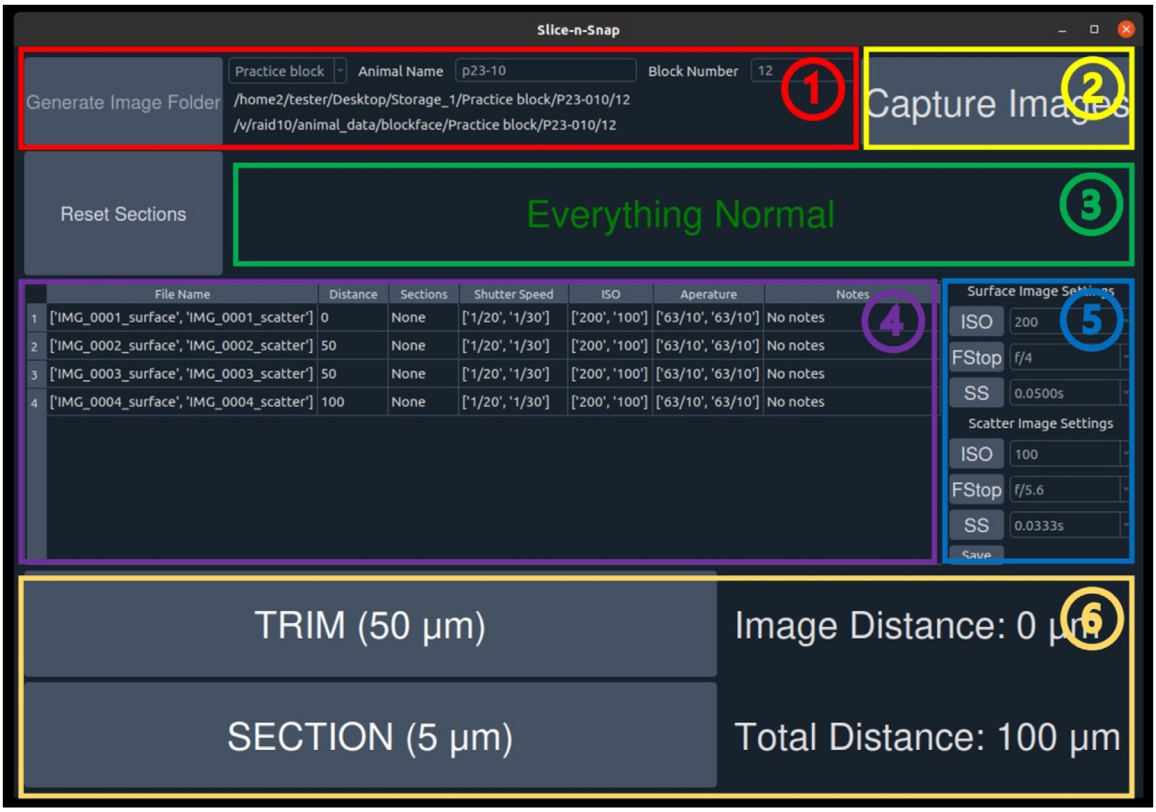

Fig. 7. The "Main Window" of the software interface. Colored numbers are provided to indicate each aspect of the software interface, with corresponding descriptions in the text.

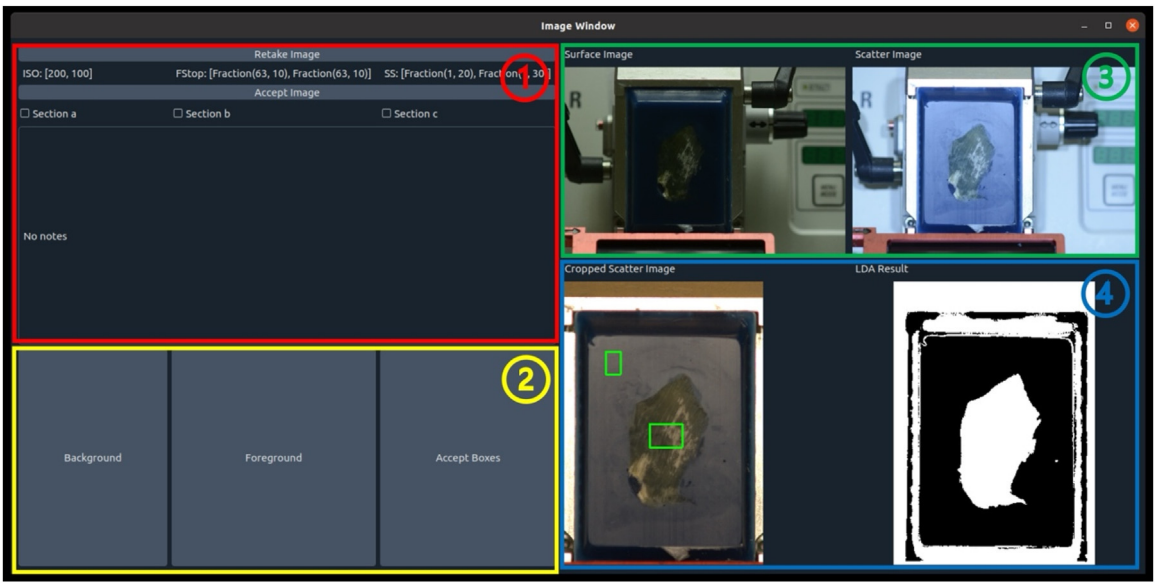

Fig. 8. The image window that is activated and shown during image capture. The different components are labeled and described in the text.

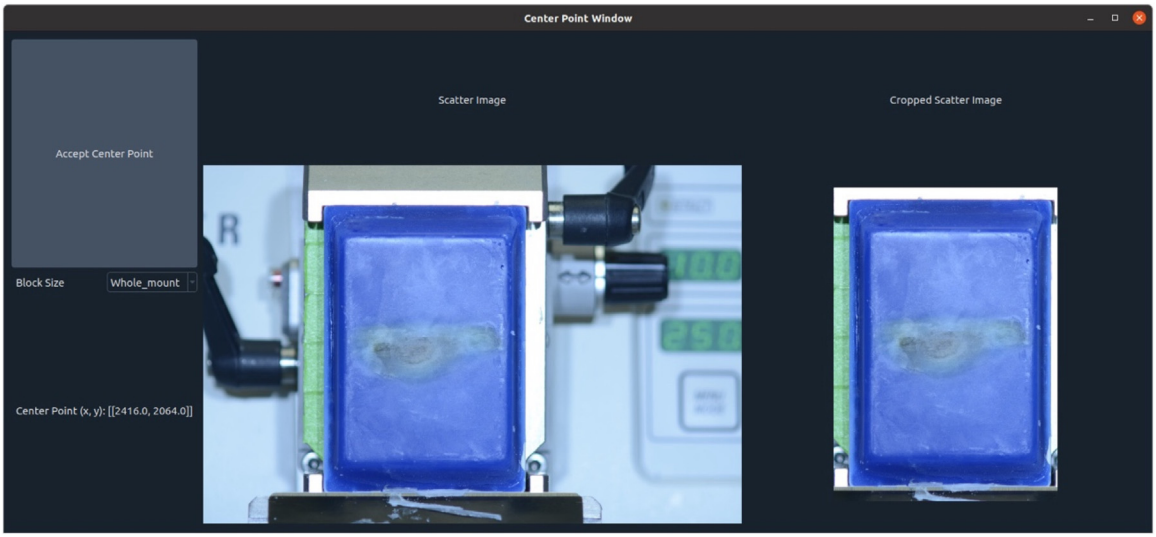

Fig. 9. An example of the center point window. The user selects the center point in the image on the left. The image on the right shows the cropped result.

processes. By clicking on the left image, the right side will show a cropped image using the clicked position as the center point. There are two cropping sizes for different blocks, "standard" and "whole mount".

The user can adjust the center point position until getting a cropped image that contains the whole block, and then click accept center point to save the position. Fig. 9 demonstrates the center point window with a cropped image.

Block face segmentation

While deep learning methods can achieve high accuracy, they require powerful GPUs to run efficiently in real-time. However, relying on a GPU-supported PC can significantly increase the economic and maintenance costs of the system. Such systems often require specific libraries, such as CUDA, to function properly, and these libraries are typically complex and require specialized expertise to operate effectively. Considering our specific use case, where the aim of the segmentation is to help operators evaluate the quality of the capture rather than obtaining a highly accurate segmentation mask, we opted to use Linear Discriminant Analysis (LDA) [19] for the task. This choice allows us to bypass the GPU requirement and achieve real-time segmentation results on a CPU-based machine with minimal computational resources (utilizing just 200 MB of memory).

The LDA-based segmentation method relies on references for image segmentation, and the choice of references significantly influences the final segmentation outcomes. In our evaluation, we considered three reference selection approaches: utilizing default references, choosing references solely from the initial image, and allowing the operator to adjust references as needed. While the first two methods may enhance efficiency and ease the operator's workload, the segmentation results are not as dependable as those achieved by allowing references to be adjusted dynamically during the sectioning process. In our approach, references can be modified at any point during sectioning, and if left unaltered, the previously established references will be retained. Following the establishment of references, the image undergoes division into 32,600 patches, and LDA is applied to classify each patch based on RGB values.

Method validation

To demonstrate the generalizability of the presented method, two tissue types, rabbit muscle ($N = 4$) and rat brain ($N = 6$) have been evaluated. The tissues were processed following the presented method. After agar embedding of the tissue, ex vivo MRI images were acquired (3D T1-weighted, rat brain: $0.15 \times 0.15 \times 0.4$ mm voxels, repetition time TR=14.7 ms, echo time TE=5.83 ms, flip angle 15°, rabbit muscle: $0.5 \times 0.5 \times 1.0$ mm, TR=6.6 ms, TE=2.24 ms, flip angle 20°, 3T Vida, Siemens). Excised rabbit tissues were grossed immediately after ex vivo MR imaging was completed. Note the rat brains did not undergo tissue grossing since a whole rat brain can fit into a standard tissue cassette. After the tissue is processed and embedded in the paraffin block, we used the presented system and acquisition protocol to obtain the sequence of block face images and sections of the block. All sections were stained with hematoxylin and eosin (H&E) and digitally scanned at 5x magnification (AxioScan.Z1, Zeiss) for image processing.

Registration of the ex vivo MR images to the block face images was achieved through reconstruction of the block face volume through utilization of the obtained physical distances during sectioning (X, Y: 0.023 mm/pixel, Z: 0.05 mm/image). After segmentation of both the ex vivo and block face volumes, we used the "General Registration" model in 3D Slicer [20] to perform volume-based affine registration. The settings include a percentage of samples of 0.9, initialize transform mode set to "useMomentsAlign", and registration phases set to "Affine".

The registration process from H&E to block face involved utilizing a 2D thin-plate spline registration method. To ensure accurate alignment, several to dozens of corresponding points in the two images were identified based on their features. To facilitate this,

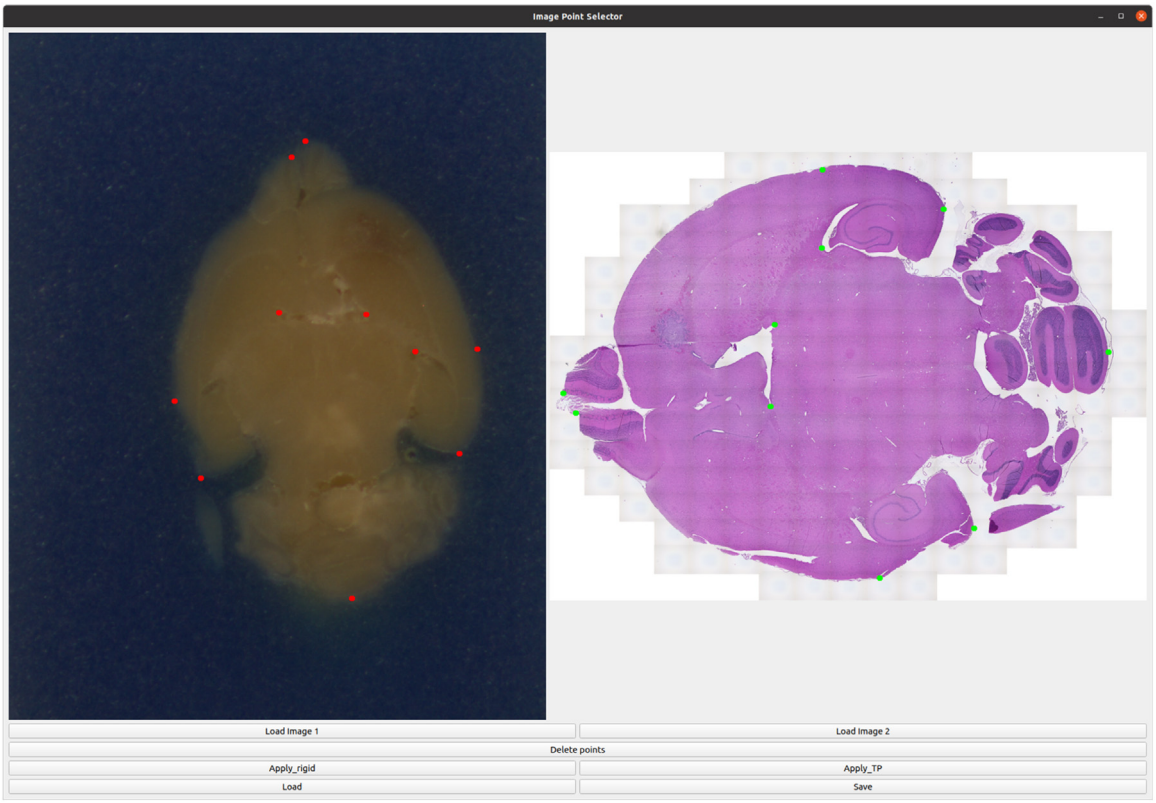

Fig. 10. GUI for H&E to block face image registration allowing users to select corresponding points in the block face (right image, red dots) and the H&E image (left image, green dots).

we developed a graphical user interface (GUI) allowing users to select correspondences from the input images. We utilized the "createThinPlateSplineShapeTransformer" function from the OpenCV library to compute the thin-plate spline registration matrix. A demonstration of our GUI is depicted in Fig. 10.

Segmentation result

Even though our data collection environment described above remains consistent with all acquisitions, variations in specific variables including color changes, lighting and paraffin to tissue contrast are seen during sectioning. Fig. 11 illustrates some of these variations and the segmentation results across rabbit muscles, and rat brains. The green boxes indicate the references selected for the segmentation. The flexibility of the LDA-based segmentation method provides robust results of the segmented tissue despite these varying conditions.

To highlight the importance of affording operator's flexibility in adjusting references, we performed a comparative analysis, examining the DICE coefficient in segmentation results. We compared the DICE coefficient between using default references and permitting the operator to modify references as needed. Furthermore, we contrasted the DICE coefficient of results obtained by selecting references solely from the initial acquisition image with the approach of enabling the operator to modify references as necessary. The DICE for the default references was found to be 0.602 compared to 0.561 when using references from the initial image only.

It is evident that both the default references and those selected solely from the initial image yield inferior segmentation results compared to the approach implemented in our software, which allows operators to modify references as necessary. These findings are consistent with our observations in Fig. 11, where variations in tissue and background colors may occur throughout the section. If the references are not updated in these images, the segmentation may not work as accurately as possible. Such results affirm the necessity of permitting operators to modify references during the sectioning process.

Block face image and 2D histology to MRI registration

Fig. 12 shows the volume-based affine registration results for ex vivo MR images to block face volumes of both rabbit muscle and rat brain tissue. The figure presents volume-rendered blocks, accompanied by individual orthogonal projections for each face.

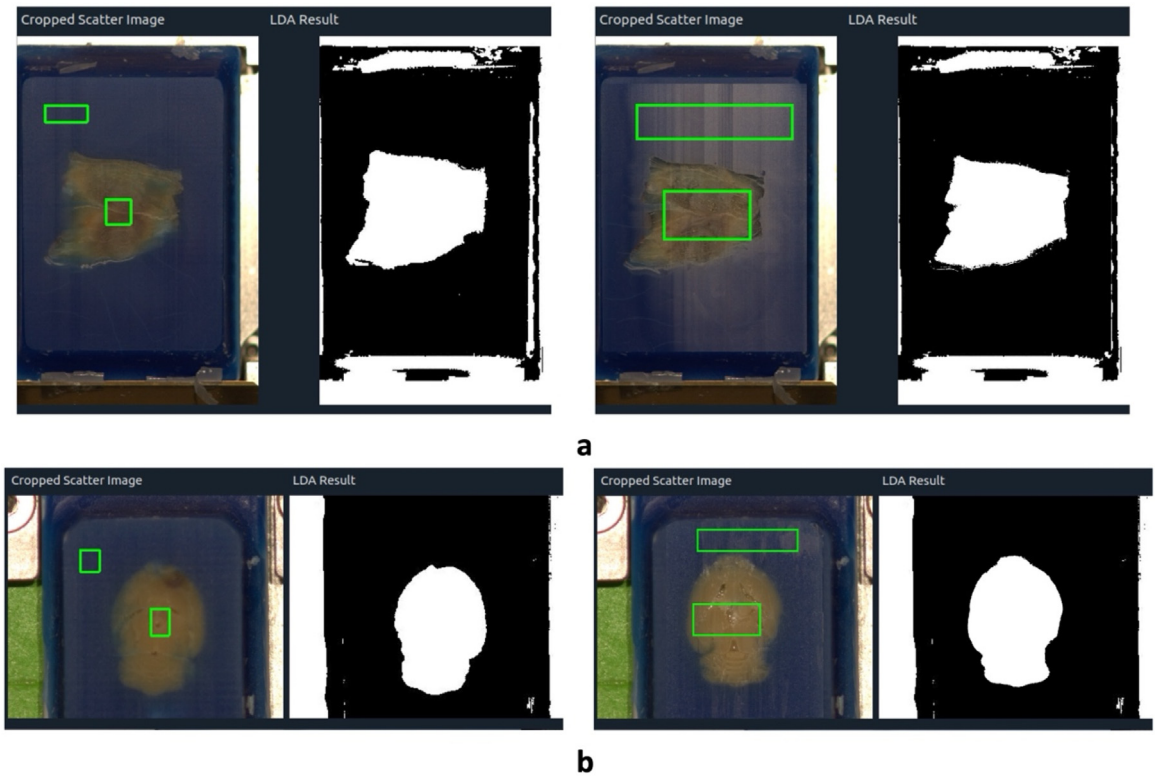

Fig. 11. Segmentation results of the boundary of tissue and paraffin utilizing the LDA technique under different image acquisition quality in both (a) rabbit muscle and (b) rat brain examples. In both cases, the LDA segmentation technique is robust despite the tissue and paraffin wax color variations as well as the selection of the patches for LDA segmentation.

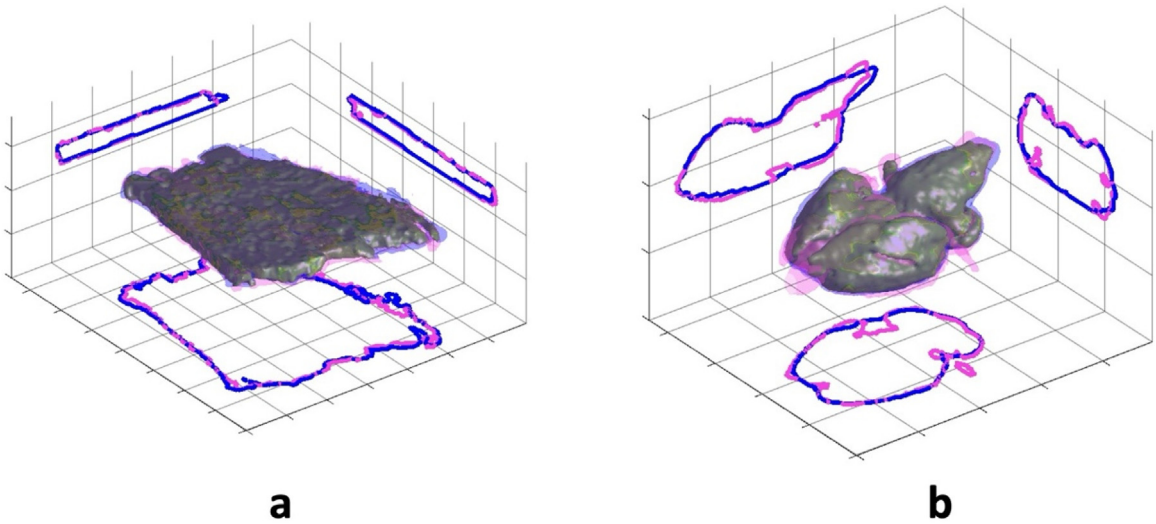

Fig. 12. Volume registration results for ex vivo MRI and block face images for (a) rabbit muscle and (b) rat brain tissues. The pink outlines are ex vivo MRI and the blue outlines are the block face segmented volumes. Grid spacing is 6 mm.

A single slice of image registration results through the volumetric registration for both rabbit muscle and rat brain are shown in Fig. 13. A checkerboard display between the block face image and ex vivo MRI is utilized to show the qualitative alignment of the two image types. Similarly, the H&E to block face registration results are shown in a checkerboard in Fig. 14. Utilizing the block face volume as an intermediary, the ex vivo slice transformation was applied to the corresponding H&E for each tissue, as illustrated in Fig. 15.

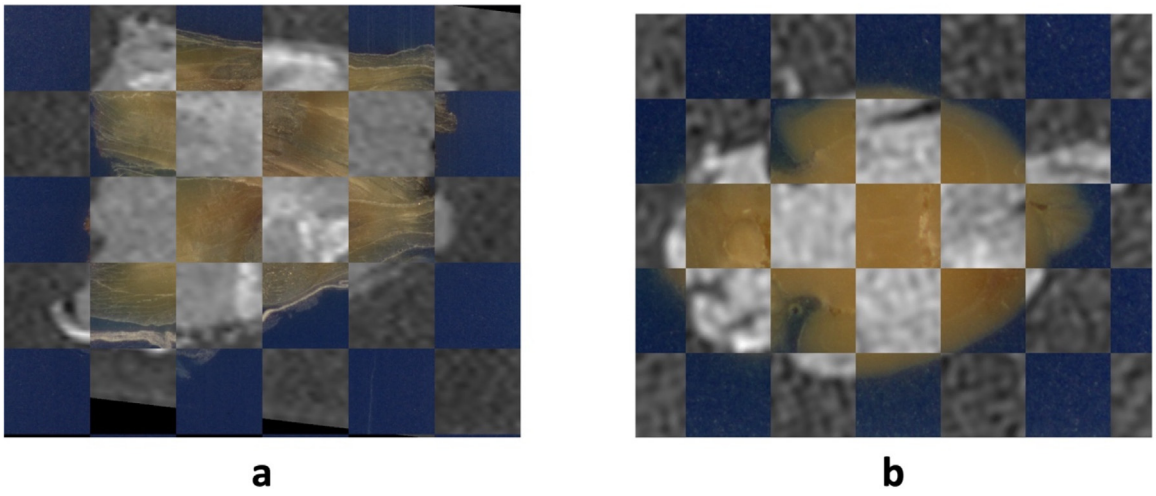

Fig. 13. Single slice plane registration results between ex vivo T1-weighted MRI and block face imaging for (a) rabbit muscle and (b) rat brain.

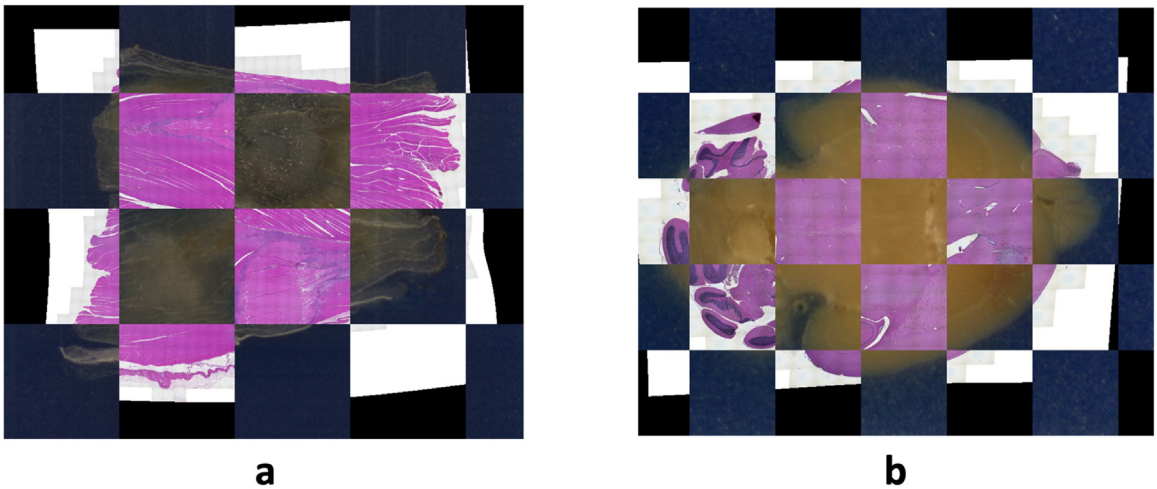

Fig. 14. H&E to block face registration results shown for a single slice in both (a) rabbit muscle and (b) rat brain.

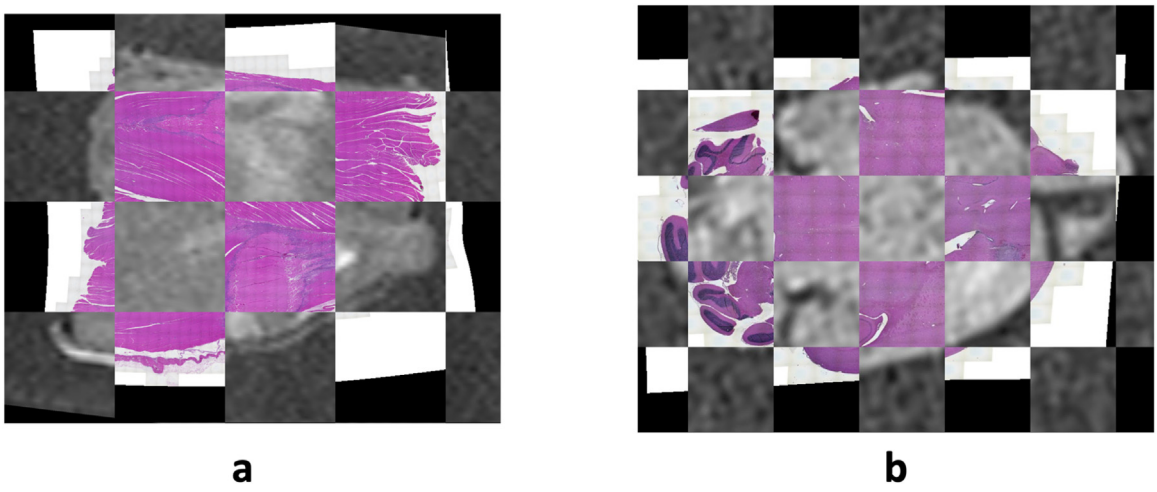

Fig. 15. Ex vivo T1-weighted MRI to H&E registration results for a single slice in both (a) rabbit muscle and (b) rat brain.

Limitations

While we have opted for a highly contrasting color (blue) as the background, accurately locating the edge line of the tissue remains challenging at times not only due to edge detection, but the reflection from the agar surface. The combination of these issues can result in a margin of error of approximately 0.1 mm in the edge area. Additionally, in instances where the tissue lacks hydration, certain part of the tissue may easily detach, posing challenges for the subsequent reconstruction process. As the proposed pipeline relies heavily on the block face as a crucial step for registration, its clinical application poses challenges due to the limited availability of tissue blocks in clinical settings.

Ethics statements

All animal data shown in this work was performed until the National Institutes of Health guide for the care and use of laboratory animals. All rats were male, while the rabbit data was equally distributed between both male and female sexes. Because this work was technology development and validation, the influence of sex is not significant.

Declaration of competing interest

The authors declare that they have no known competing financial interests or personal relationships that could have appeared to influence the work reported in this paper.

CRediT authorship contribution statement

Mingzhen Shao: Methodology, Software, Validation, Investigation, Writing – original draft, Visualization. **Amanpreet Singh:** Methodology, Software, Writing – review & editing. **Sara Johnson:** Conceptualization, Methodology, Writing – review & editing. **Alissa Pessin:** Investigation, Methodology, Writing – review & editing. **Robb Merrill:** Methodology, Resources, Writing – review & editing. **Ariana Page:** Investigation, Methodology, Writing – review & editing. **Henrik Odéen:** Writing – review & editing, Funding acquisition. **Sarang Joshi:** Conceptualization, Methodology, Software, Resources, Writing – review & editing, Supervision, Project administration, Funding acquisition. **Allison Payne:** Conceptualization, Methodology, Software, Resources, Writing – review & editing, Supervision, Project administration, Funding acquisition.

Data availability

Data will be made available on request.

Acknowledgments

The authors acknowledge the direct financial support for the research reported in this publication provided by the Huntsman Cancer Foundation and the Experimental Therapeutics Program at Huntsman Cancer Institute and an Institutional Research Grant, IRG-21–131–01, from the American Cancer Society. The authors also acknowledge support by the National Institutes of Health's National Cancer Institute under Award Numbers P30CA042014, R37CA224141, R01CA259686, NIH Office of the Director under Award Numbers S10OD018482 and S10OD026788, and National Institute of Biomedical Imaging and Bioengineering under Award Number R21EB033638.

References

[1] C.M.C. Tempany, N.J. McDannold, K. Hynynen, F.A. Jolesz, Focused ultrasound surgery in oncology: overview and principles, Radiology. 259 (1) (2011) 39–56.
[2] S.J.C.G. Hectors, I. Jacobs, C.T.W. Moonen, G.J. Strijkers, K. Nicolay, MRI methods for the evaluation of high intensity focused ultrasound tumor treatment: current status and future needs, Magn. Reson. Med. 75 (1) (2016) 302–317.
[3] S.-W. Yoon, S.H. Cha, Y.G. Ji, H.C. Kim, M.H. Lee, J.H. Cho, Magnetic resonance imaging-guided focused ultrasound surgery for symptomatic uterine fibroids: estimation of treatment efficacy using thermal dose calculations, Eur. J. Obstetric. Gynecol. Reproduct. Biol. 169 (2) (2013) 304–308.
[4] J.D. Hazle, R.J. Stafford, R.E. Price, Magnetic resonance imaging-guided focused ultrasound thermal therapy in experimental animal models: correlation of ablation volumes with pathology in rabbit muscle and VX2 tumors, J. Magnetic Resonance Imag. 15 (2) (2002) 185–194.
[5] R.B. Sequeiros, J. Kariniemi, R. Ojala, L. Chengli, M. Haapea, A.B. Sequeiros, O. Tervonen, Liver tumor laser ablation–increase in the subacute ablation lesion volume detected with post procedural MRI, Acta Radiol. 51 (5) (2010) 505–511.
[6] J. Pichat, J.E. Iglesias, T. Yousry, S. Ourselin, M. Modat, A survey of methods for 3D histology reconstruction, Med. Image Anal. 46 (2018) 73–105.
[7] C. Orczyk, H. Rusinek, A.B. Rosenkrantz, A. Mikheev, F.-M. Deng, J. Melamed, S.S. Taneja, Preliminary experience with a novel method of three-dimensional co-registration of prostate cancer digital histology and in vivo multiparametric MRI, Clin. Radiol. 68 (12) (2013) e652–e658.
[8] L. Dickinson, Y. Hu, H.U. Ahmed, C. Allen, A.P. Kirkham, M. Emberton, D. Barratt, Image-directed, tissue-preserving focal therapy of prostate cancer: a feasibility study of a novel deformable magnetic resonance-ultrasound (MR-US) registration system, BJU Int. 112 (5) (2013) 594–601.
[9] M. Goubran, S. de Ribaupierre, R.R. Hammond, C. Currie, J.G. Burneo, A.G. Parrent, T.M. Peters, A.R. Khan, Registration of in-vivo to ex-vivo MRI of surgically resected specimens: a pipeline for histology to in-vivo registration, J. Neurosci. Method. 241 (2015) 53–65.
[10] M. Rusu, W. Shao, C.A. Kunder, J.B. Wang, S.J.C. Soerensen, N.C. Teslovich, R.R. Sood, L.C. Chen, R.E. Fan, P. Ghanouni, Registration of presurgical MRI and histopathology images from radical prostatectomy via RAPSODI, Med. Phys. 47 (9) (2020) 4177–4188.
[11] L. Li, S. Pahwa, G. Penzias, M. Rusu, J. Gollamudi, S. Viswanath, A. Madabhushi, Co-Registration of ex vivo surgical histopathology and in vivo T2 weighted MRI of the prostate via multi-scale spectral embedding representation, Sci. Rep. 7 (1) (2017) 1–12.
[12] A. Losnegård, L. Reisæter, O.J. Halvorsen, C. Beisland, A. Castilho, L.P. Muren, J. Rørvik, A. Lundervold, Intensity-based volumetric registration of magnetic resonance images and whole-mount sections of the prostate, Comput. Med. Imag. Graphic. 63 (2018) 24–30.

[13] J.E. Iglesias, M. Modat, L. Peter, A. Stevens, R. Annunziata, T. Vercauteren, E. Lein, B. Fischl, S. Ourselin, Alzheimer's Disease Neuroimaging Initiative, Joint registration and synthesis using a probabilistic model for alignment of MRI and histological sections, Med. Image Anal. 50 (2018) 127–144.
[14] W. Shao, L. Banh, C.A. Kunder, R.E. Fan, S.J.C. Soerensen, J.B. Wang, N.C. Teslovich, N. Madhuripan, A. Jawahar, P. Ghanouni, J.D. Brooks, G.A. Sonn, M. Rusu, ProsRegNet: a deep learning framework for registration of MRI and histopathology images of the prostate, Med. Image Anal. 68 (2021) 101919.
[15] R.R. Sood, W. Shao, C. Kunder, N.C. Teslovich, J.B. Wang, S.J.C. Soerensen, N. Madhuripan, A. Jawahar, J.D. Brooks, P. Ghanouni, R.E. Fan, G.A. Sonn, M. Rusu, 3D Registration of pre-surgical prostate MRI and histopathology images via super-resolution volume reconstruction, Med. Image Anal. 69 (2021) 101957.
[16] A. Ruchti, A. Neuwirth, A.K. Lowman, S.R. Duenweg, P.S. LaViolette, J.D. Bukowy, Homologous point transformer for multi-modality prostate image registration, PeerJ. Comput. Sci. 8 (2022) e1155.
[17] B.E. Zimmerman, S.L. Johnson, H.A. Odéen, J.E. Shea, R.E. Factor, S.C. Joshi, A.H. Payne, Histology to 3D in vivo MR registration for volumetric evaluation of MRgFUS treatment assessment biomarkers, Sci. Rep. 11 (1) (2021) 18923.
[18] A.G. Atkins, X. Xu, G. Jeronimidis, Cutting, by 'pressing and slicing,' of thin floppy slices of materials illustrated by experiments on cheddar cheese and salami, J. Mater. Sci. 39 (2004) 2761–2766, doi:10.1023/B:JMSC.0000021451.17182.86.
[19] A.J. Izenman, Linear discriminant analysis, in: Modern Multivariate Statistical Techniques: Regression, Classification, and Manifold Learning, Springer, New York, 2008, pp. 237–280.
[20] R. Kikinis, S.D. Pieper, K.G. Vosburgh, 3D Slicer: a platform for subject-specific image analysis, visualization, and clinical support, in: F.A. Jolesz (Ed.), Intraoperative Imaging and Image-Guided Therapy, 2014, pp. 277–289.